JCSE Journal of Computing Science and Engineering

Regular Paper

Journal of Computing Science and Engineering,
Vol. 15, No. 1, March 2021, pp. 34-46

Automated Detection of Age-Related Macular Degeneration from OCT Images Using Multipath CNN

Anju Thomas, P. M. Harikrishnan, Adithya K. Krishna, P. Palanisamy, and Varun P. Gopi*

Department of Electronics and Communication Engineering, National Institute of Technology Tiruchirappalli, Tamilnadu, India

anjukandathil.thomas@gmail.com, haripm033@gmail.com, adithya.krishnakumar@gmail.com, palan@nitt.edu, varun@nitt.edu

Abstract

Age-related macular degeneration (AMD) is an eye disorder that can have harmful effects on older people. AMD affects the macula, which is the core portion of the retina. Hence, early diagnosis is necessary to prevent vision loss in the elderly. To this end, this paper proposes a novel multipath convolutional neural network (CNN) architecture for the accurate diagnosis of AMD. The architecture proposed is a multipath CNN with five convolutional layers used to classify AMD or normal images. The multipath convolution layer enables many global structures to be generated with a large filter kernel. In this proposed network, the sigmoid function is used as the classifier. The proposed CNN network is trained on the Mendeley dataset and evaluated on four datasets—the Mendeley, OCTID, Duke, and SD-OCT Noor datasets—and it achieved accuracies of 99.60%, 99.61%, 96.67%, and 93.87%, respectively. Although the proposed model is only trained on the Mendeley dataset, it achieves good detection accuracy when evaluated with other datasets. This indicates that the proposed model has the capacity to detect AMD. These results demonstrate the efficiency of the proposed algorithm in detecting AMD compared to other approaches. The proposed CNN can be applied in real-time due to its reduced complexity and learnable parameters.

Category: Computer Graphics / Image Processing

Keywords: Age-related macular degeneration; Multipath CNN; Sigmoid; Macular region

I. INTRODUCTION

The retina in the human eye contains a photo sensitive layer of optic nerve tissue that protects the eyeball's inner surface. This layer receives the centered light through the focal point and moves into neural signs over it. The macula is the main area that lies in the central part of the retina, and is used for sensing. It includes unique photoreceptor nerve cell layers that are responsible for detecting color, light intensity, and subtle visual information [1]. The main eye diseases that occur in the retina are drusen, choroidal neovascularization (CNV), age-related macular degeneration (AMD), and diabetic macular edema (DME). These eye conditions are among the most prevalent causes of vision loss in Western nations, and cases are estimated to number 300 million worldwide within the next few years [2]. Such diseases can cause blindness and affect patients' lives. In response to this, scientists have been compelled to build a modern and efficient tool for diagnosing certain diseases in these circumstances. One

Open Access http://dx.doi.org/10.5626/JCSE.2021.15.1.34 http://jcse.kiise.org

Received 24 December 2020; **Accepted** 12 March 2021

*Corresponding Author

 pISSN: 1976-4677 eISSN: 2093-8020

of the imaging techniques called OCT, which is based on weak coherence light interference, detects the back reflection at various biological tissue levels of incoming weak coherent light or several scattered signals. Therefore, the cellular tissues with two or three-dimensional structural representation can be obtained by scanning, which is similar to ultrasonography displaying cross-sectional images. Medical image analysis was developed from the1970s to the 1990s with the sequential application of low-level pixel processing and mathematical modeling to create systems that could solve specific tasks. Next, the pattern recognition or machine learning process has gained popularity and has come to form the basis of many commercially available successful medical image analysis systems. As more learning algorithms continue to emerge, computers can now learn to interpret medical images. This idea has caused many deep learning algorithmic models (networks) to be created, and they consist of many layers that turn input images into classified outputs while learning increasingly deeper characteristics [3]. The convolutional neural network (CNN) technique is a state-of-the-art deep learning technique for medical disease diagnosis, particularly for databased on X-ray images and OCT images. To a limited extent, CNN has several layers that transform their input with the convolutional layer. While computer vision has been revolutionized by deep learning, its implementation remains limited because of the lack of broad training sets. It is always essential to provide a large training set before deep learning can be effectively used [4]. The macular region is a vital area of the retina characterized by fine vision, color identification, and other visual capabilities. When a lesion occurs in the macular region, the vision will be adversely affected.

AMD is the progression of the macular region's aging, which occurs for most people over 45 years old, and AMD incidence rate increases with age, making it one of the oldest significant causes of visual impairment. The prevalence of AMD in 2016 was 170 million people, and it is projected to have reached 196 million in 2020 and 288 million by 2040 [5]. The disorder evolves into one of two states: neovascular ("wet") AMD and regional atrophy ("late dry") AMD. CNV splits through the neovascular AMD via the neural retina, thereby releasing liquids, lipids, and blood, resulting in fibrous scarring. These advanced forms of illness cause the most serious vision loss from AMD. Thus, early detection is a critical aspect of the treatment of AMD. OCT provides us with a clear view of the nine retinal layers, as shown in Fig. 1 [6], whose varying thickness and irregularities encode a lot of information that can help diagnose diseases, such as CNV, DME, and drusen [7-11]. AMD can be in one of two forms, namely, dry AMD (drusen) and wet AMD (choroidal neo vascularization).

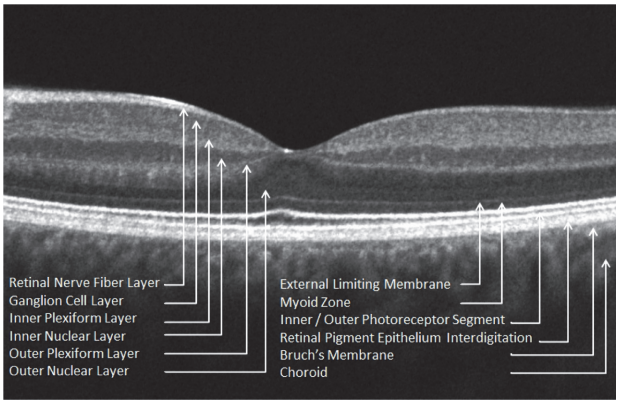

Fig. 1. A healthy OCT B scan of retina with all the layers marked [11].

A. Drusen

Drusen, also called dry AMD, which is histologically classified as hard formations, consists of small hyaline deposits with delimited margins which are considered age-related low-risk changes. Soft drusen, which are deposits of granular or amorphous material, are considered precursors to AMD. Drusen can progress to an atrophic form (dry) or an exudative form (wet) of AMD. The risk is based on the lesion number, size, and confluence of drusen. A color SD-OCT image of drusen is shown in Fig. 2 [12]. In the case of drusen, there are corrugations present in the RPE+Bruch's membrane layer.

B. Choroidal Neovascularization

CNV is also called wet AMD, which involves the growth of new blood vessels. The vessels originate from the choroid through a break in Bruch's membrane into the sub-retinal pigment epithelium or subretinal space. CNV is a major cause of vision loss; statistics show that 10% of AMD patients are affected by the wet form [13]. A color SD-OCT image of CNV is shown in Fig. 3 [14].

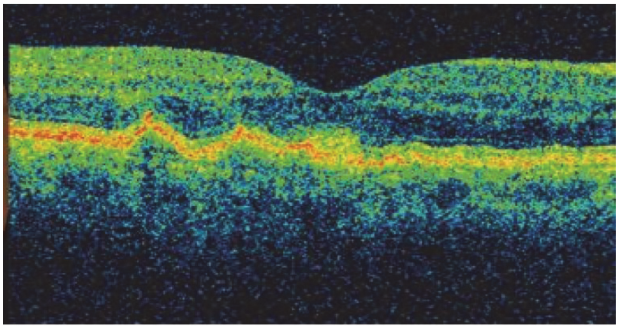

Fig. 2. Drusen is characterized by the corrugations observed in the RPE+Bruch's membrane layers,which has very high reectance, shown as reddish pixels [12].

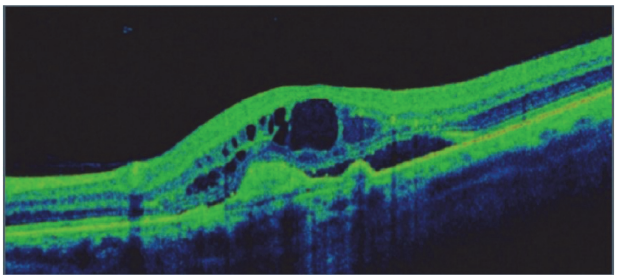

Fig. 3. Color SD-OCT image of CNV [14].

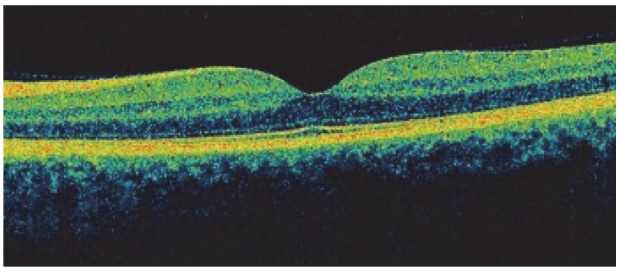

Fig. 4. Color SD-OCT image of Normal [12].

C. Normal or Healthy

Fig. 4 shows the color SD-OCT of a normal eye. This paper proposes novel deep CNN architecture that can be used to automate the accurate diagnose of AMD in the early stage. The main features of this work are:

1. The multipath feature extraction permits the CNN to merge more features regarding the sparse local and fine global structures.
2. The 128 relevant features from the second fully connected layer of the CNN are followed by the sigmoid activation function for the binary classification.
3. The proposed network is trained using the Mendeley dataset and tested with the Mendeley dataset as well as the other three datasets, which provide notable results.
4. Suitable for real-time implementation due to the reduced number of learnable parameters, which reduces the complexity of the system.

II. RELATED WORK

Srinivasan et al. [15] worked on the Duke SD-OCT dataset, which consists of 15 AMD and 15 healthy OCT image. The feature extraction was performed using a multiscale histogram of oriented gradient (HOG) descriptor. Then, the features were classified using a support vector machine (SVM) classifier with leave-3-out cross-validation. They used a threshold value of 33%, where if 33% or more images in the volume show abnormality, then only that volume was classified as diseased; ultimately, they achieved an overall accuracy of 93.3%. In [16], the Gaussian filter was used for noise removal. The retinal pigment epithelium (RPE) layer was segmented using the estimated line value of RPE (ELRPE) from the denoised images. A combination of ELRPE and new estimated line of RPE (NERPE) was used to remove the retinal nerve fiber layer (RNFL). They used the Duke SD-OCT dataset [15]. The main limitation of this method is that it cannot work on images with a significant amount of noise. Farsiu et al. [1] introduced a semi-automatic segmentation of Bruch's membrane (BM), inner limiting membrane (ILM), and RPE layers. The features were extracted manually. Linear regression was used to separate AMD and healthy images with leave-1-out cross-validation. The area under curve (AUC) was used to measure the system's performance, and they obtained a value of 0.99. The Bioptigen SD-OCT images were used in the experiment (Bioptigen, Morrisville, NC, USA). Precise retinal layer segmentation and manual corrections were required to avoid misleading outcomes. Naz et al. [17] worked on the Duke dataset to classify AMD and normal images. RPE layer extraction was performed using intensity-based thresholding. The layer was smoothed by a curve fitting method. An SVM classifier with 10-fold cross-validation was adopted for the classification, and it obtained an overall accuracy of 96%. In that study, they remarked that the eye curvature estimation using 2nd-degree polynomial affects detection in images with many drusen. The work used only a tiny portion of the original dataset. One study recommended the use of local configurable patterns (LCP) using a correlation-based feature subset selection algorithm to extract features from the OCT images [18]. The sequential minimal optimization (SMO) method was used to classify the images. The work was done using the Duke dataset and it achieved 96.6% accuracy. The OCT image was first scaled, then divided into a spatial pyramid by using the multiscale spatial pyramid (MSSP). In [19], the authors used the Duke dataset. They selected the region of interest (ROI) from those images with a size of 512×256. Then, the speckle noise in the images was eliminated using kernel regression. In the denoised image, intensity-based thresholding was used to extract the RPE layer by removing the RNFL layers. Polynomial fitting was used to obtain the best fit line for the data. The overall accuracy was 92%, but the sensitivity was 0.56. Karri et al. [20] used the CNN model to classify images into AMD and normal images.Transfer learning using GoogLeNet was proposed, and it achieved an overall accuracy of 94% on the Duke dataset. For the Heidelberg Spectralis dataset classification, a modified version of the VGG-16 CNN model was used in [21]. That network had 21 layers and obtained an accuracy of 93.4%. Sun et al. [22] suggested a dictionary learning method in which the

images were divided into three different scales. In each patch, the local features were measured, such as scale-invariant feature transform (SIFT), and the features' sparse representation was concatenated into vectors to create a global representation. The linear SVM was used as the classifier to classify the input images, and it acquired an overall accuracy of 96.6% on the Duke dataset. Kaymak and Serener [23] used the Mendeley dataset, which consisted of 37,206 CNV, 8,616 drusen, and 51,140 normal images for training and 750 images for testing. The transfer learning model was then trained and tested on the OCT images, and it obtained an overall accuracy of 96.53%. In [23], the original AlexNet was trained, and a deep network was generated based on the trained AlexNet. The Mendeley dataset [24] was used to evaluate the network's performance, and it showed an accuracy of 98.26%. A three-dimensional segmentation methodology was adopted to segment the SD-OCT in [25]. Three features were extracted, such as the volume of hyper-reflective intra-retinal spots (HIS), drusen, and the myoid zone-ellipsoid zone (MZ-EZ) boundary curvature. A random forest classifier was employed, and 97.7% accuracy was attained on the Duke dataset. The main limitation of this Work was that the retinal layer segmentation failed to detect in cases of extreme pathologies. Rasti et al. [26] proposed a classification network that worked on the Noor SD-OCT dataset and the Duke dataset. All images were resized to 496×512, and the image intensity values were normalized to 0 mean and one standard deviation. Then, the eye was flattened and the background was cropped. Different CNN classifiers were used, and the results of each were combined using a Gaussian mixture model (GMM). The network achieved AUC values of 0.999 for the Duke dataset and 0.998 for the SD-OCT Noor dataset. The main highlights were that a GMM model was used to find the optimal classifier. The spatial pyramid helped reduce the time and prevent overfitting. An eighteen-layer recombined residual CNN was proposed in [27]; the main advantage of this was that there combined residual CNN showed better results than the original residual network. A CNN-based classification model was suggested in [28]. Before classification, sparse representation-based image denoising, accompanied by thresholding and morphological operation, was used. The network was trained and tested on the Duke and private datasets, and it respectively obtained AUC values of 0.9856 and 0.9783. Kuwayama et al. [29] tested the network on a dataset obtained from Nagoya City University Graduate School of Medical Sciences (consisting of 570 normal images and 136 wet AMD images). Due to a lack of data, augmentation was performed. A CNN model was used for classification; after parameter tuning, the network obtained 85% accuracy, which was a lower value. In [30], the work was done on the publicly available dataset, namely the Project macula dataset, which consists of the OCT and fundus images. The input images were manually cropped to select the desired area in the image. The data augmentation was performed to increase the dataset. Transfer learning with VGG-19 was adopted in this work. The VGG- 19 network has 16 convolutional layers and three fully connected layers, and it was pre-trained on the ImageNet dataset. Here, transfer learning was used to extract relevant features from the input images, and finally, these features were fed into a random forest classifier. This method achieved an overall accuracy in OCT classification of 82.6% and an AUC value of 0.906. Fang et al. [4] introduced an iterative fusion CNN network; the network consisted of two sections: a basic CNN section and a network fusion section. Here, VGG - 16 is used as the basic CNN network. In the fusion section, multiple layers of information are iteratively incorporated. Hwang et al. [31] was scheduled to work on private and Mendeley datasets. The private dataset consisted of OCT images of 174 healthy and 583 AMD patients. The private dataset was augmented to obtain a large dataset and ensure that the resolution and image sizes were similar to the original data. The author tried three different CNN networks for the classification ResNet-50, Inception-v3, and VGG-16; 80% of the data were applied for training while the remaining 20% were used to validate the networks. The models were verified using another independent dataset and the Mendeley dataset. The Inception-v3 model shows the best performance over the Mendeley dataset, with 96.93% accuracy. The ResNet-50 and VGG-16 attained accuracies of 95.87% and 91.20%, respectively, on the Mendeley dataset. Serener and Serte [32] used pre-trained AlexNet and ResNet for the classification of dry and wet AMD. The AUC value in AlexNet was 0.81, and that for the 18-layer ResNet was 0.94 for dry AMD classification. For wet AMD classification, AlexNet and ResNet had respective AUC values of 0.61 and 0.63, respectively. In [33], a guided convolutional neural network (LGCNN) was introduced for the classification of retinal OCT images. To produce the retinal layer segmentation maps, ReLayNet wasused, and two lesion-related retinal layers were extracted. The two sub-networks were used to extract the information present in the layers. The outputs of two sub-networks were combined using a fully connected layer, then produced the final output prediction. The authors utilized a private dataset and the Mendeley dataset. The overall accuracy achieved with the Mendeley dataset was 93.96%. Das et al. [34] used a multiscale deep feature fusion (MDFF) network for classification [34]. The Mendeley dataset was used for training and testing. The system had three main stages of operation, namely preprocessing, multiscale feature extraction, and classification. The preprocessing stage focused on removing the retina's curvature by using a graph-based curvature method, then selecting the desired ROI for further analysis. The multiscale CNN network was used

to extract the coarse features from OCT images. Then, finally, the different multiscale layers were fused to classify the images. The whole system produced an overall accuracy of 97.71%. The imbalance in the dataset is controlled during classifier learning by implementing a cost-sensitive loss function. This work represented one of the best existing algorithms for OCT classification. Yim et al. [35] worked on a real-time dataset, which contained 11 months of patient data, to create the prediction system for finding wet AMD. Two deep learning networks were used: segmentation and classification (ensemble deep learning model).The specificity of the network was 0.90. The author created a system that predicted wet AMD conversion risk within 6 months. A 19-layer CNN network was proposed in [36] for AMD classification. The network was trained on the Mendeley, Duke, and private datasets, and it achieved an accuracy of 95.3%.

Bhatia et al. [37] developed Pegasus OCT software based on theVGG-16 basic building blocks. The system was trained and tested using three publicly available (the Duke, Mendeley, and SD-OCT Noor datasets) and three private datasets. The overall AUC value of AMD classification was 0.99. AMD classification using fundus and OCT images was proposed in [38]. Two transfer learning networks using ResNet-50 were developed, one for fundus and other for OCT images. Each network's last stage has 2048 features, and these features are concatenated and ultimately given to a fully connected stage before being classified. The network was tested using 143 fundus and OCT image pairs. The main limitation of this work was the limited dataset.

III. MODEL

A CNN contains several computational layers, such as the convolutional layer (CL), pooling layer (PL), and fully connected layer (FCL), to extract features from input images and classify them into different classes. Previous studies have demonstrated the use of a conventional CNN in detecting AMD from OCT images due to its effective high-level feature extraction [39]. This paper brings forth a new CNN architecture for the classification of AMD in OCT images. The proposed CNN applies a multipath feature extraction method that helps the network create global structures.

IV. IMPLEMENTATION

The proposed CNN architecture is shown in Fig. 5. In the proposed CNN, the input size is 200×200; this is the most reliable scale. As the input size reaches 200, the precision does not improve significantly, and the computational time increases. In addition, the precision is reduced when the input image size is less than 200. When the input dimension is reduced in medical images, particularly in OCT and fundus images, significant information is lost. As a result, the image input size was set to 200 times 200. The proposed CNN consists of five CL. The extraction scheme for multipath features provides an additional path to combine features created from early layers and later layers to maintain losses in the later layers of global structures (e.g., object or contour shape). The proposed neural network contains four successive single-scale convolutional layers (SSCL) with one

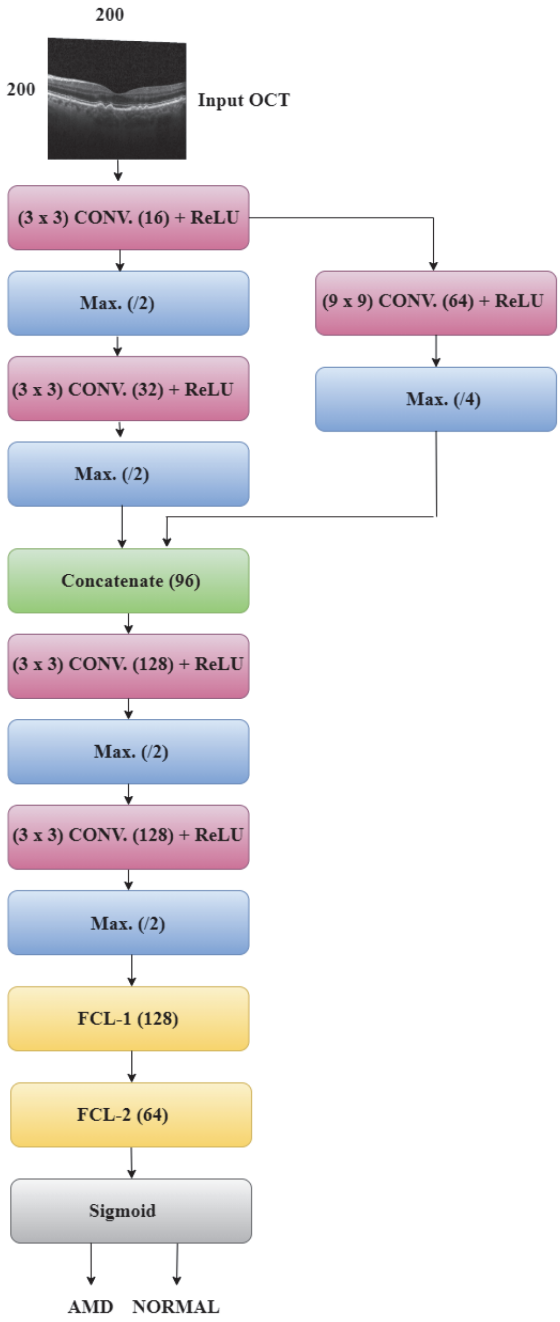

Fig. 5. Proposed CNN architecture.

multipath convolutional layer (MPCL) and two FCLs. The first SSCL uses a filter size of 3×3 and generates 16 feature maps that are given to the MPCL with the filter size of 9×9 to extract global features from the OCT images. The first SSCL is followed by a max-pool layer of kernel size 2×2 with stride 2. The max-pool values are given to another SSCL with the same filter size of 3×3 and generates 32 feature maps to the next max-pool layer. Eventually, all paths from SSCL and MPCL are combined using the concatenation layer, thus producing 96 feature maps. The result is then given to two SSCL having a filter size of 3×3 with 128 feature maps each. The max-pooling layers are used to lower the spatial resolution of the following layers of the network, so the max-pool layer is used after all CL. The pooling method the network to learn from inputs to more complex local structures. The first fully connected layer with 128 neurons has activated only 64 neurons to the next level. Because of the complete connectivity structure, the denser fully connected layer frequently leads to overfitting. Herein, a dropout scheme [40] is applied to the proposed architecture to the first and second fully connected layers with a dropout ratio of 0.5 to prevent overfitting. The predicted results are normalized using the sigmoid function, which is good for binary classification in the logistic regression model. The sigmoid function maps every individual value between 0 and 1 [41]. Sigmoid is used to map predictions to probabilities in machine learning, as given below,

$$Sigmoid\ (x) = \frac{1}{1+e^{-x}} \tag{1}$$

where x is the input to the function. The rectified linear unit (ReLU) is used to activate each CL. ReLU suppresses all values less than zero to 0, there by retaining all values greater than zero. Compared to the sigmoid and the tanh activation function, the ReLU displays greater gradient changes [42]. It is also simple to implement, and it can help boost training speed efficiency and network inference.

A. Multipath Convolution Layer

The extraction of multipath features enables more robust features to be combined with sparse local features and fine global structures. The fine global structures are extracted using earlier CLs in the network. The derived features become more sparse and localized after the network propagates to the deeper layer in which the global architectures are reduced. The suggested multipath function avoids the global structure losses by taking the shortcut. The network consists of one MPCL shortcut path, in that one parallel CL with filter size 9×9 generates 64 feature maps. A max-pool layer with stride four is introduced into the shortcut to combine the functionalities of the two branches. Depth-wise concatenation is used to merge feature maps generated from these two branches. The network cannot describe the global structure through an SSCL. The application of large filter sizes can cover the global structures due to the improved coverage area. The proposed CNN extends an SSCL to an MPCL, thereby enabling the network to produce more global structures with large filter dimensions

B. Model Training Parameters

The proposed CNN architecture is trained using backpropagation [43] with a batch size of 32. Stochastic gradient descent (SGD) [44], is used to train the CNN. The default settings for the CNN model are as follows: learning rate $\alpha = 0.001$, exponential decay rates $\beta_1 = 0.9$, $\beta_2 = 0.999$, and numerical value $\epsilon = 10^{-8}$, epochs = 50. SGD with momentum is used very frequently due to its stability and good convergence, although it converges slower than the other optimization algorithms. The total number of learn able parameters in the proposed CNN is 1,993,249.

C. Evaluation

The results of the proposed work are evaluated based on the confusion matrix [45-48]. Table 1 presents the structure of the confusion matrix that depicts a binary classifier's characteristics. In that matrix, the numbers of true positives (TP), false negatives (FN), false positives (FP), and true negatives (TN) are M, N, O, and P, respectively. TP and TN give properly classified data results while FP and FN give the wrongly classified information. We can measure the precision, F1-score, recall, and accuracy using these values to analyze machine performance.

$$Accuracy = \frac{P+M}{O+P+N+M} \tag{2}$$

The false positive rate (FPR) refers to the number of false positive outcomes. For a good classifier, the best FPR rate is 0.

$$FPR = \frac{P}{O+P} \tag{3}$$

The positive value of prediction is given by precision. This value provides details about how effectively our system is avoiding FPs. It can be measured as follows:

Table 1. Binary-classification confusion matrix

		Predicted class	
		Normal	**AMD**
Targeted class	Normal	M	N
	AMD	O	P

$$Precision = \frac{M}{M+N} \quad (4)$$

Recall, also referred to as sensitivity, provides information about how effectively the model decreases FN. That can be measured as

$$Recall = \frac{M}{M+O} \quad (5)$$

The F1-score specifies the harmonic mean of precision and recall

$$F1-score = \frac{2M}{2M+O+N} \quad (6)$$

The proposed method is implemented in the Keras framework in Python using TensorFlow. The experiment is conducted using a PC with a Nvidia GeForce, RTX 2080 11GB GPU.

D. Dataset

The proposed network is trained and validated using the Mendeley dataset [24], given in Table 2. The Mendeley dataset contains 500 AMD images (250 dry AMD and 250 wet AMD) and 250 normal images for testing. We have also tested the same model with the other three datasets, namely the OCTID [49], Duke dataset [15], and SD-OCT Noor dataset [26]. The details of the data distribution are provided in Table 3.

E. Performance Analysis

1) Mendeley Dataset

The confusion matrix of the Mendeley dataset [24] is presented in Table 4. The testing dataset consists of 250 dry AMD, 250 wet AMD, and 250 normal images, so here we took a total of 500 AMD images and 250 normal images for testing. Out of 500 AMD images, only two images are misclassified as normal. In normal images, only one image out of 250 is misclassified as AMD.

Table 2. Data distribution for training and validation

	Training (90%)		Validation (10%)	
	AMD	Normal	AMD	Normal
Mendeley dataset	41,238	46,026	4,583	5,114

Table 3. Data distribution for testing

	Testing	
	AMD	Normal
Mendeley dataset [24]	500	250
OCTID [49]	55	206
Duke dataset [15]	15	15
SD-OCT Noor dataset [26]	48	50

Table 5. Confusion matrix of Mendeley dataset

		Predicted class	
		Normal	AMD
Targeted class	Normal	498	2
	AMD	1	249

Table 5. Classwise values of evaluation parameter of network on Mendeley dataset [24]

	Precision	Recall	F1-score	Accuracy (%)	AUC
AMD	0.9980	0.9960	0.9947	99.6	-
Normal	0.9920	0.9960	0.9947	99.6	-
WA	0.9960	0.9960	0.9960	99.6	0.999

The classwise and weighted average (WA) performance of the network on the Mendeley dataset are listed in Table 5. The WA evaluation parameters such as F1-score, recall, and precision are greater than 0.99. For a good network, the AUC is nearer to 1. The proposed network attained an AUC value of 0.9998 in the Mendeley dataset [24]. Hence, this indicates that the proposed network performs well in AMD/normal classification.

A comparison of the proposed method with existing methods is provided in Table 6. In the case of the Mendeley dataset, it achieved an accuracy of 99.6%, which is the one of the highest accuracies among the compared works. Kaymak and Serener [23] proposed AlexNet, which is highly sensitive to the training dataset. The AlexNet obtained 98.26% accuracy and an AUC of 0.9917 with 800 epochs. The other previous works achieved less than 98% accuracy and an AUC value under 0.992. The ROC curves of all the previous results and the proposed work are plotted in Fig. 6. Based on the ROC curve, it is clear that the proposed work has the best performance of all compared works. The proposed network is trained only on the Mendeley dataset, but it is

Table 6. Comparison of proposed work with existing works conducted on Mendeley dataset [24]

	WA accuracy	AUC
Kermany et al. [24]	0.9653	0.9762
Das et al. [34]	0.9771	0.9900
Kaymak & Serener [23]	0.9826	0.9917
Feng et al. [4]	0.9340	0.9798
Huang et al. [31]	0.9690	0.9835
Proposed method	**0.9960**	**0.9980**

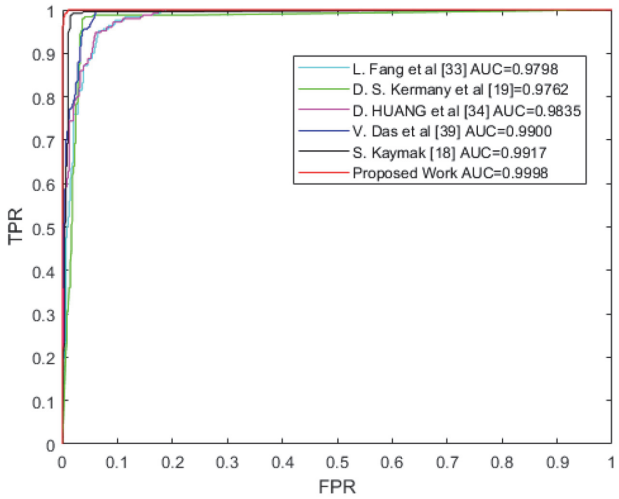

Fig. 6. ROC curves for the various architectures of deep learning using Mendeley dataset [24].

tested on other publicly available OCT datasets such as the Duke dataset [15], OCTID [49], and SD-OCTNoor dataset [26], and their performance is provided below.

1) Duke Dataset

The Duke dataset [15] consists of 30 image volumes where in 15 are AMD and the remaining 15 are normal. The confusion matrix of the Duke dataset is listed in Table 7. All AMD patients are classified correctly, and only one healthy case is misclassified as AMD. The performance evaluation of the Duke dataset is tabulated in Table 8. All the AMD patients are classified properly, and the model obtained 100% accuracy in AMD patient detection. One misclassification in normal leads to an accuracy value of 93.33%. The overall accuracy of the Duke dataset is 96.66% while the AUC value is 1.

A comparison of the Duke dataset results with existing methods is presented in Table 9. With the Duke dataset

Table 7. Confusion matrix of Duke dataset [15]

		Predicted class	
		Normal	**AMD**
Targeted class	Normal	15	0
	AMD	1	14

Table 8. The evaluation parameter of network on Duke dataset [15]

	Precision	**Recall**	**F1-score**	**Accuracy**	**AUC**
AMD	0.9375	1.0000	0.9677	1.0000	-
Normal	1.0000	0.9333	0.9655	0.9333	-
WA	0.9687	0.9666	0.9666	0.9661	1.000

Table 9. Comparison of proposed work with existing works conducted on Duke dataset [24]

	WA accuracy	**AUC**
Srinivasan et al. [15]	0.933	-
Khalid et al. [19]	0.920	-
Hussain et al. [25]	**0.977**	0.9900
Wang et al. [18]	0.966	0.9910
Meng et al. [27]	0.9666	-
Sun et al. [22]	0.9666	-
Proposed method	**0.9667**	**1.000**

[15], the proposed method achieved an accuracy of 0.96 using 5-CL with a sigmoid activation function. In [25], the authors achieved an accuracy of 0.977 using 15-fold cross-validation. This method failed to detect disease in cases of extreme pathologies. The overall accuracy of 0.9666 has been claimed in [27], but they used 17-CL to obtain that result. Sun et al. [22] obtained one of the best accuracies of 96.6% by using the traditional hand crafted feature extraction method. Wang et al. [18] used a correlation-based feature subset selection algorithm and achieved an AUC of 0.991.

3) SD-OCT Noor Dataset

The confusion matrix of the SD-OCT Noor dataset [26] is provided in Table 10. The dataset consists of 48 AMD patients and 50 healthy participants. Of the 48 AMD patients, the proposed method correctly predicted 45 AMD patients, with three misclassifications. In the case of normal, the real so three misclassifications, and the remaining 47 normal images are classified correctly. The network performance on the SD-OCT Noor dataset is tabulated in Table 11. The AMD patient classification accuracy is 0.9375 with three misclassifications while the

Table 10. Confusion matrix of SD-OCT Noor dataset [26]

		Predicted class	
		Normal	**AMD**
Targeted class	Normal	45	3
	AMD	3	47

Table 11. The evaluation parameter of network on SD-OCT Noor dataset [26]

	Precision	**Recall**	**F1-score**	**Accuracy**	**AUC**
AMD	0.9375	0.9375	0.9375	0.9375	-
Normal	0.9400	0.9400	0.9400	0.9400	-
WA	0.9387	0.9387	0.9387	0.9387	0.9812

Table 12. Comparison of proposed work with base work of SD-OCT Noor dataset [26]

Method	Precision	AUC
Rasti et al. [26]	0.9886	0.9980
Proposed method	0.9387	0.9387

healthy detection accuracy is 0.94; the overall accuracy of 93.87% is obtained. The comparison of the SD-OCT Noor dataset results with existing methods is given in Table 12. In [26], the authors resized all images into 496×512, then normalized the intensity values to zero mean and one standard deviation. Then, they flattened the eye and cropped the background. Different existing CNN classifiers were used, and the results of each were combined using a GMM model, and a precision rate of 0.9886 and an AUC of 0.998 were ultimately achieved.

4) OCTID

The confusion matrix is presented in Table 13. In OCTID, only 1 out of 55 AMD images is misclassified as normal, while all the normal images are classified properly. The classwise and weighted average values of the proposed method are listed in Table 14. With the OCTID dataset, the proposed model achieved an accuracy of 99.61%. It should be noted that the network produces less misclassification for all the datasets. The system's accuracy shows the best performance on a different dataset with the proposed CNN. Even if the proposed model is trained only on the Mendeley dataset, it can still achieve good detection accuracy when tested on other datasets such as the Duke, OCTID, and SD-OCT Noor datasets. This indicates that the proposed model has the ability to classify AMD/Normal images.

Table 13. Confusion matrix of OCTID dataset [49]

		Predicted class	
		Normal	AMD
Targeted class	Normal	54	1
	AMD	0	206

Table 14. The evaluation parameter of network on OCTID dataset [49]

	Precision	Recall	F1-score	Accuracy	AUC
AMD	1.0000	0.9818	0.9908	0.9818	-
Normal	0.9951	1.0000	0.9975	1.0000	-
WA	0.9961	0.9961	0.9961	0.9961	0.9980

F. Grad-Cam Images

Another satisfying observation is that the proposed network's activation is nearly the same as the color OCT images. Most of the clinical diagnoses made by ophthalmologists are based on the color OCT image in the eye.

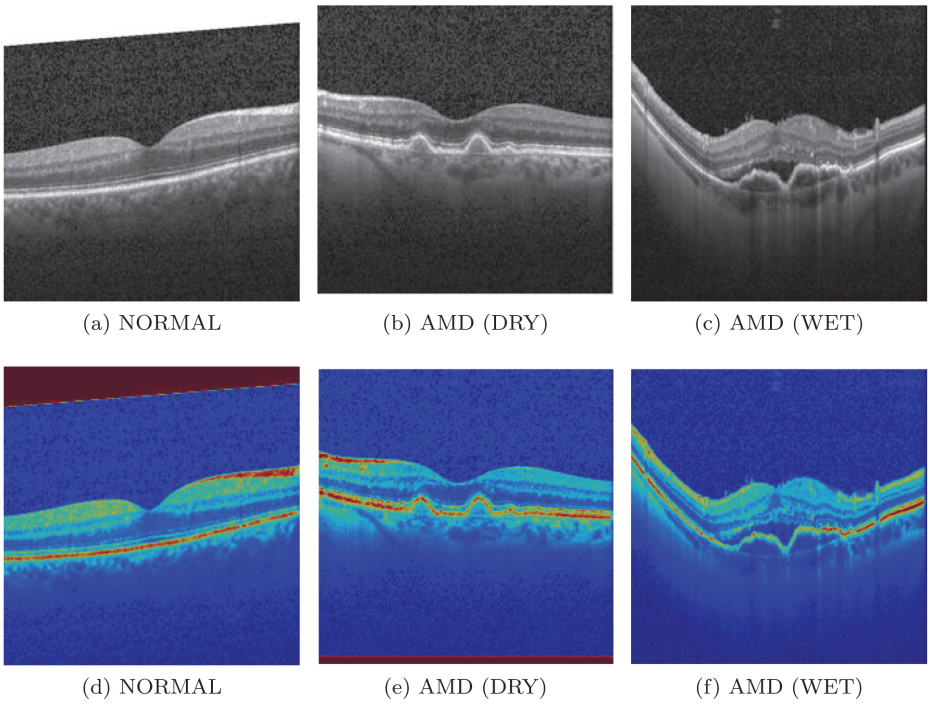

(a) NORMAL (b) AMD (DRY) (c) AMD (WET)

(d) NORMAL (e) AMD (DRY) (f) AMD (WET)

Fig. 7. Retinal images (a, b, c) and corresponding Grad-Cam images (d, e, f).

The proposed network generates a similar kind of activation map using gradient-based class activation mapping (Grad-CAM) [50, 51], from which doctors can then directly validate and classify the result generated in cases of misclassification. Grad-CAM finds the gradient of the last CL and feature maps concerning the predicted class, then backpropagates the gradient to produce eat-map of the same size as the input, when superimposed on the image, provides an idea of the discriminative regions of an image. In color OCT, the RPE+Bruch's membrane layers have very high reflectance and appear as red pixels. If one examines the activation for dry AMD in Fig. 7(e) and compares it with the color OCT image in Fig. 2, the similarity is evident. The corrugations highlighted in the activation map conform with the corrugations present later in the RPE+Bruch's membrane layer, thus justifying the decision-making process. After comparing the activation map of wet AMD in Fig. 7(f) with its color OCT in Fig. 3, it can be seen that the Bruch's membrane breaks into the subretinal pigment epithelium or subretinal space. For a normal image, the RPE+Bruch's membrane layer is almost a line, without any corrugations.

V. CONCLUSION

A novel multipath CNN architecture is proposed to automate the accurate diagnosis of AMD in the early stage. The proposed CNN has five CLs for classifying AMD or normal images. The multipath feature extraction allows the CNN to merge more features regarding the sparse local and fine global structures. In this proposed network, the sigmoid function is used as the classifier. The proposed CNN is trained on the Mendeley dataset and tested on four datasets, namely the Mendeley, OCTID, Duke, and SD-OCT Noor datasets, and it achieved respective accuracies of 99.60%, 99.61%, 96.67%, and 93.87%. Even if the proposed model is trained only on the Mendeley dataset, it still achieves good detection accuracy when tested with other datasets. This indicates the proposed model's ability to classify AMD/normal images from other datasets. A comparison with other approaches shows the efficiency of the proposed algorithm in detecting AMD. The proposed architecture can be applied in rapid screening of the eye for the early detection of AMD. Due to the reduced complexity and fewer learnable parameters, the proposed CNN can be implemented in real-time.

ACKNOWLEDGMENTS

The authors would like to thank Dr. S Sujatha of the Institute of Ophthalmology, Joseph Eye Hospital, Tiruchirappalli, India for her valuable guidance throughout this research.

This research work is funded by Science and Engineering Research Board (SERB), Government of India (No. SERB/F/11639/2018-2019 dated February 26, 2019).

REFERENCES

1. S. Farsiu, S. J. Chiu, R. V. O'Connell, F. A. Folgar, E. Yuan, J. A. Izatt, et al., "Quantitative classification of eyes with and without intermediate age-related macular degeneration using optical coherence tomography," *Ophthalmology*, vol. 121, no. 1, pp. 162-172, 2014.
2. Y. Kanagasingam, A. Bhuiyan, M. D. Abramoff, R. T. Smith, L. Goldschmidt, and T. Y. Wong, "Progress on retinal image analysis for age related macular degeneration," *Progress in Retinal and Eye Research*, vol. 38, pp. 20-42, 2014.
3. G. Litjens, T. Kooi, B. E. Bejnordi, A. A. A. Setio, F. Ciompi, M. Ghafoorian, J. A. W. M. van der Laak, B. van Ginneken, and C. I. Sanchez, "A survey on deep learning in medical image analysis," *Medical Image Analysis*, vol. 42, pp. 60-88, 2017.
4. L. Fang, Y. Jin, L. Huang, S. Guo, G. Zhao, and X. Chen, "Iterative fusion convolutional neural networks for classification of optical coherence tomography images," *Journal of Visual Communication and Image Representation*, vol. 59, pp. 327-333, 2019.
5. W. L. Wong, X. Su, X. Li, C. M. G. Cheung, R. Klein, C. Y. Cheng, and T. Y. Wong, "Global prevalence of age-related macular degeneration and disease burden projection for 2020 and 2040: a systematic review and meta-analysis," *The Lancet Global Health*, vol. 2, no. 2, pp. e106-e116, 2014.
6. J. Oakley, "The eye as a window to the central nervous system," 2014, https://www.voxeleron.com/optical-coherence-tomography-imaging-diseases-central-nervous-system/.
7. G. Trichonas and P. K. Kaiser, "Optical coherence tomography imaging of macular oedema," *British Journal of Ophthalmology*, vol. 98, no. Suppl 2, pp. ii24-ii29, 2014.
8. A. Giovannini, G. P. Amato, C. Mariotti, and B. Scassellati-Sforzolini, "OCT imaging of choroidal neovascularisation and its role in the determination of patients' eligibility for surgery," *British Journal of Ophthalmology*, vol. 83, no. 4, pp. 438-442, 1999.
9. A. Garcia-Layana, C. Ciuffo, J. Zarranz-Ventura, and A. Alvarez-Vidal, "Optical coherence tomography in age-related macular degeneration," 2017, https://amdbook.org/book/export/html/423.
10. K. M. Jemshi, V. P. Gopi, and S. I. Niwas, "Development of an efficient algorithm for the detection of macular edema from optical coherence tomography images," *International Journal of Computer Assisted Radiology and Surgery*, vol. 13, no. 9, pp. 1369-1377, 2018.
11. A. Thomas, A. P. Sunija, R. Manoj, R. Ramachandran, S. Ramachandran, P. G. Varun, and P. Palanisamy, "RPE layer detection and baseline estimation using statistical methods and randomization for classification of AMD from retinal OCT," *Computer Methods and Programs in Biomedicine*, vol. 200, article no. 105822, 2020. https://doi.org/10.1016/

j.cmpb.2020.105822
12. G. Coscas, *Optical Coherence Tomography in Age-Related Macular Degeneration*. Heidelberg, Germany: Springer, 2009.
13. M. D. Davis, R. E. Gangnon, L. Y. Lee, L. D. Hubbard, B. E. Klein, R. Klein, et al., "The Age-Related Eye Disease Study severity scale for age-related macular degeneration: AREDS report No. 17," *Archives of Ophthalmology*, vol. 123, no. 11, pp. 1484-1498, 2005.
14. A. T. H. Dumar and J. D. Arias, "Choroidal Neovascularization: OCT Angiography Findings," 2020, https://eyewiki.aao.org/Choroidal_Neovascularization:_OCT_Angiography_Findings.
15. P. P. Srinivasan, L. A. Kim, P. S. Mettu, S. W. Cousins, G. M. Comer, J. A. Izatt, and S. Farsiu, "Fully automated detection of diabetic macular edema and dry age-related macular degeneration from optical coherence tomography images," *Biomedical Optics Express*, vol. 5, no. 10, pp. 3568-3577, 2014.
16. J. Sugmk, S. Kiattisin, and A. Leelasantitham, "Automated classification between age-related macular degeneration and diabetic macular edema in OCT image using image segmentation," in *Proceedings of the 7th 2014 Biomedical Engineering International Conference*, Fukuoka, Japan, 2014, pp. 1-4.
17. S. Naz, A. Ahmed, M. U. Akram, and S. A. Khan, "Automated segmentation of RPE layer for the detection of age macular degeneration using OCT images," in *Proceedings of 2016 6th International Conference on Image Processing Theory, Tools and Applications (IPTA)*, Oulu, Finland, 2016, pp. 1-4.
18. Y. Wang, Y. Zhang, Z. Yao, R. Zhao, and F. Zhou, "Machine learning based detection of age-related macular degeneration (AMD) and diabetic macular edema (DME) from optical coherence tomography (OCT) images," *Biomedical Optics Express*, vol. 7, no. 12, pp. 4928-4940, 2016.
19. S. Khalid, M. U. Akram, A. Jameel, and T. Khalil, "Automated detection of drusens to diagnose age related macular degeneration using OCT images," *International Journal of Computer Science and Information Security*, vol. 14, no. 10, pp. 1-5, 2016.
20. S. P. K. Karri, D. Chakraborty, and J. hatterjee, "Transfer learning based classification of optical coherence tomography images with diabetic macular edema and dry age-related macular degeneration," *Biomedical Optics Express*, vol. 8, no. 2, pp. 579-592, 2017.
21. C. S. Lee, D. M. Baughman, and A. Y. Lee, "Deep learning is effective for classifying normal versus age-related macular degeneration OCT images," *Ophthalmology Retina*, vol. 1, no. 4, pp. 322-327, 2017.
22. Y. Sun, S. Li, and Z. Sun, "Fully automated macular pathology detection in retina optical coherence tomography images using sparse coding and dictionary learning," *Journal of Biomedical Optics*, vol. 22, no. 1, article no. 016012, 2017. https://doi.org/10.1117/1.JBO.22.1.016012
23. S. Kaymak and A. Serener, "Automated age-related macular degeneration and diabetic macular edema detection on oct images using deep learning," in *Proceedings of 2018 IEEE 14th International Conference on Intelligent Computer Communication and Processing (ICCP)*, Cluj-Napoca, Romania, 2018, pp. 265-269.
24. D. S. Kermany, M. Goldbaum, W. Cai, C. C. Valentim, H. Liang, S. L. Baxter, et al., "Identifying medical diagnoses and treatable diseases by image-based deep learning," *Cell*, vol. 172, no. 5, pp. 1122-1131, 2018.
25. M. A. Hussain, A. D. Bhuiyan, C. Luu, R. H. Theodore Smith, R. Guymer, H. Ishikawa, J. S. Schuman, and K. Ramamohanarao, "Classification of healthy and diseased retina using SD-OCT imaging and Random Forest algorithm," *PloS One*, vol. 13, no. 6, article no. e0198281, 2018. https://doi.org/10.1371/journal.pone.0198281
26. R. Rasti, H. Rabbani, A. Mehridehnavi, and F. Hajizadeh, "Macular OCT classification using a multi-scale convolutional neural network ensemble," *IEEE Transactions on Medical Imaging*, vol. 37, no. 4, pp. 1024-1034, 2018.
27. T. Meng, C. Wu, T. Jia, Y. Jiang, and Z. Jia, "Recombined convolutional neural network for recognition of macular disorders in SD-OCT images," in *Proceedings of 2018 37th Chinese Control Conference (CCC)*, Wuhan, China, 2018, pp. 9362-9367.
28. Y. Rong, D. Xiang, W. Zhu, K. Yu, F. Shi, Z. Fan, and X. Chen, "Surrogate-assisted retinal OCT image classification based on convolutional neural networks," *IEEE Journal of Biomedical and Health Informatics*, vol. 23, no. 1, pp. 253-263, 2018.
29. S. Kuwayama, Y. Ayatsuka, D. Yanagisono, T. Uta, H. Usui, A. Kato, N. Takase, Y. Ogura, and T. Yasukawa, "Automated detection of macular diseases by optical coherence tomography and artificial intelligence machine learning of optical coherence tomography images," *Journal of Ophthalmology*, vol. 2019, article no. 6319581, 2019. https://doi.org/10.1155/2019/6319581
30. T. K. Yoo, J. Y. Choi, J. G. Seo, B. Ramasubramanian, S. Selvaperumal, and D. W. Kim, "The possibility of the combination of OCT and fundus images for improving the diagnostic accuracy of deep learning for age-related macular degeneration: a preliminary experiment," *Medical & Biological Engineering & Computing*, vol. 57, no. 3, pp. 677-687, 2019.
31. D. K. Hwang, C. C., Hsu, K. J. Chang, D. Chao, C. H. Sun, Y. C. Jheng, et al., "Artificial intelligence-based decision-making for age-related macular degeneration," *Theranostics*, vol. 9, no. 1, pp. 232-245, 2019.
32. A. Serener and S. Serte, "Dry and wet age-related macular degeneration classification using OCT images and deep learning," in *Proceedings of 2019 Scientific Meeting on Electrical-Electronics & Biomedical Engineering and Computer Science (EBBT)*, Istanbul, Turkey, 2019, pp. 1-4.
33. L. Huang, X. He, L. Fang, H. Rabbani, and X. Chen, "Automatic classification of retinal optical coherence tomography images with layer guided convolutional neural network," *IEEE Signal Processing Letters*, vol. 26, no. 7, pp. 1026-1030, 2019.
34. V. Das, S. Dandapat, and P. K. Bora, "Multi-scale deep feature fusion for automated classification of macular pathologies from OCT images," *Biomedical Signal Processing and Control*, vol. 54, article no. 101605, 2019. https://doi.org/10.1016/j.bspc.2019.101605
35. J. Yim, R. Chopra, T. Spitz, J. Winkens, A. Obika, C. Kelly, et al., "Predicting conversion to wet age-related macular degeneration using deep learning," *Nature Medicine*, vol. 26,

no. 6, pp. 892-899, 2020.
36. A. M. Alqudah, "AOCT-NET: a convolutional network automated classification of multiclass retinal diseases using spectral-domain optical coherence tomography images," *Medical & Biological Engineering & Computing*, vol. 58, no. 1, pp. 41-53, 2020.
37. K. K. Bhatia, M. S. Graham, L. Terry, A. Wood, P. Tranos, S. Trikha, and N. Jaccard, "Disease classification of macular optical coherence tomography scans using deep learning software: validation on independent, multicenter data," *Retina*, vol. 40, no. 8, pp. 1549-1557, 2020.
38. Z. Xu, W. Wang, J. Yang, J. Zhao, D. Ding, F. He, et al., "Automated diagnoses of age-related macular degeneration and polypoidal choroidal vasculopathy using bi-modal deep convolutional neural networks," *British Journal of Ophthalmology*, vol. 105, no. 4, pp. 561-566, 2020.
39. J. H. Tan, S. V. Bhandary, S. Sivaprasad, Y. Hagiwara, A. Bagchi, U. Raghavendra, et al., "Age-related macular degeneration detection using deep convolutional neural network," *Future Generation Computer Systems*, vol. 87, pp. 127-135, 2018.
40. N. Srivastava, G. Hinton, A. Krizhevsky, I. Sutskever, and R. Salakhutdinov, "Dropout: a simple way to prevent neural networks from overfitting," *The Journal of Machine Learning Research*, vol. 15, no. 1, pp. 1929-1958, 2014.
41. J. Milgram, M. Cheriet, and R. Sabourin, ""One against one" or "one against all": Which one is better for handwriting recognition with SVMs?," in Proceedings of the 10th *International Workshop on Frontiers in Handwriting Recognition*, La Baule, France, 2006.
42. A. Krizhevsky, I. Sutskever, and G. E. Hinton, "ImageNet classification with deep convolutional neural networks," *Advances in Neural Information Processing Systems*, vol. 25, pp. 1097-1105, 2012.
43. J. Bouvrie, "Notes on convolutional neural networks," 2006, http://cogprints.org/5869/.
44. L. Bottou, "Stochastic gradient descent tricks," in *Neural Networks: Tricks of the Trade*. Heidelberg, Germany: Springer, 2012, pp. 421-436.
45. S. Visa, B. Ramsay, A. L. Ralescu, and E. Van Der Knaap, "Confusion matrix-based feature selection," in *Proceedings of the 22nd Midwest Artificial Intelligence and Cognitive Science Conference (MAICS)*, Cincinnati, OH, 2011, pp. 120-127.
46. S. Gayathri, A. K. Krishna, V. P. Gopi, and P. Palanisamy, "Automated binary and multiclass classification of diabetic retinopathy using haralick and multiresolution features," *IEEE Access*, vol. 8, pp. 57497-57504, 2020.
47. S. Gayathri, V. P. Gopi, and P. Palanisamy, "A lightweight CNN for diabetic retinopathy classification from fundus images," *Biomedical Signal Processing and Control*, vol. 62, article no. 102115, 2020. https://doi.org/10.1016/j.bspc.2020.102115
48. S. Gayathri, V. P. Gopi, and P. Palanisamy, "Automated classification of diabetic retinopathy through reliable feature selection," *Physical and Engineering Sciences in Medicine*, vol. 43, no. 3, pp. 927-945, 2020.
49. P. Gholami, P. Roy, M. K. Parthasarathy, and V. Lakshminarayanan, "OCTID: optical coherence tomography image database," *Computers & Electrical Engineering*, vol. 81, article no. 106532, 2020. https://doi.org/10.1016/j.compeleceng.2019.106532
50. R. R. Selvaraju, M. Cogswell, A. Das, R. Vedantam, D. Parikh, and D. Batra, "Grad-cam: visual explanations from deep networks via gradient-based localization," in *Proceedings of the IEEE International Conference on Computer Vision*, Venice, Italy, 2017, pp. 618-626.
51. M. Raju, V. P. Gopi, V. S. Anitha, and K. A. Wahid, "Multi-class diagnosis of Alzheimer's disease using cascaded three dimensional-convolutional neural network," *Physical and Engineering Sciences in Medicine*, vol. 43, no. 4, pp. 1219-1228, 2020.

Anju Thomas https://orcid.org/0000-0002-2178-0531

Anju Thomas received the B. Tech. degree in Electronics and Communication Engineering from Vimal Jyothi Engineering College, Kannur University, Kerala, India, in 2015, and the M. Tech. degree in Communication Engineering and Signal Processing from Government Engineering College Wayanad affiliated with APJ Abdul Kalam Technological University, India, in 2018. She is currently pursuing Ph.D. in Image Processing from the Department of Electronics and Communication Engineering at National Institute of Technology, Tiruchirappalli, India. Her research interests include biomedical signal processing, sensor signal processing, image & video processing, machine learning, and computer vision.

P. M. Harikrishnan https://orcid.org/0000-0003-1844-9503

P. M. Harikrishnan received B.E. degree in Electronics and Communication Engineering from Shree Devi Institute of Technology Mangalore, Karnataka, India affiliated to Visvesvarayya Technological University Belagavi, Karnataka, India in 2013 and M.Tech. in Communication Engineering and Signal Processing from Government of Engineering College Wayanad affiliated to APJ Abdul Kalam Technological University, Trivandrum, India in 2017. He is currently pursuing Ph.D. in Image and Video Processing from the Department of Electronics and Communication Engineering at National Institute of Engineering Tiruchirappalli, Tamilnadu, India. His research interests include computer vision, video processing, image processing and deep learning. He is currently working as Senior Research Fellow in the Department of Electronics and Communication Engineering, National Institute of Engineering Tiruchirappalli, Tamilnadu, India.

Adithya K. Krishna https://orcid.org/0000-0002-2284-703X

Adithya K. Krishna is currently pursuing the B.Tech. degree in Electronics and Communication Engineering with the National Institute of Technology at Tiruchirappalli, Tiruchirappalli, India. His research interests include signal processing, medical image processing, computer vision, machine learning, and deep learning.

P. Palanisamy https://orcid.org/0000-0003-3687-5944

P. Palanisamy graduated B.E. degree in Electronics and Communication Engineering from Bharathiar University, Coimbatore, Tamil Nadu, India and M.E. degree in (Communication systems) and Ph.D. degree in the area of Signal Processing from National Institute of Technology, Tiruchirappalli, India. He worked as a Scientific Officer in the Department of Electronics, Govt. of India, sponsored research project at National Institute of Technology, Tiruchirappalli from March 1997 to July 1998. Since July, 1998, he has been with National Institute of Technology, Tiruchirappalli as a regular Faculty in the Department of Electronics and Communication Engineering. Currently he is a Professor in the Department of Electronics and Communication Engineering, National Institute of Technology, Tiruchirappalli, India. His area of interest includes image processing, medical image analysis, data and image compression, statistical signal processing, array signal processing, detection and bearing estimation, etc.

Varun P. Gopi https://orcid.org/0000-0001-5593-3949

Varun P. Gopi received the B.Tech. Degree in Electronics and Communication Engineering from Amal Jyothi College of Engineering, Kanjirappally, India affiliated to Mahatma Gandhi University, Kottayam, India in 2007 and the M.Tech. in Signal Processing from College of Engineering Trivandrum, affiliated to Kerala University, Trivandrum, India in 2009. He pursued his Ph.D. in Medical image processing from the Department of Electronics and Communication Engineering, National Institute of Technology (NIT), Tiruchirappalli, India in 2014. He is a recipient of the Canadian Commonwealth Scholarship Award-2011-12 under Graduate Student Exchange Program in the Department of Electrical and Computer Engineering, University of Saskatchewan, Saskatoon, SK, Canada. Currently, he is working as an Assistant Professor in the Department of Electronics and Communication Engineering, NIT Tiruchirappalli, Tamilnadu, India. His area of interest includes signal processing, medical image processing, artificial intelligence, augmented reality in healthcare, IoT in healthcare, computer vision, etc.